J Mater Sci (2014) 49:2035–2044
DOI 10.1007/s10853-013-7892-6

Thermo-mechanical properties of innovative microcrystalline cellulose filled composites for art protection and restoration

Annalisa Cataldi · Andrea Dorigato · Flavio Deflorian · Alessandro Pegoretti

Received: 12 September 2013 / Accepted: 13 November 2013 / Published online: 27 November 2013

Abstract Microcrystalline cellulose (MCC) powder was selected as a natural reinforcement for a commercial acrylic adhesive widely used in the field of art protection and restoration (Paraloid B72). In particular, various amounts (from 5 to 30 wt%) of MCC were melt compounded with Paraloid B72 to prepare new thermoplastic polymer composites for the cultural heritage conservation field. Scanning electron microscopy showed that MCC flakes are uniformly dispersed within the matrix at all the tested compositions, without preferential orientation. Thermogravimetric analysis evidenced an increase of thermal stability due to the MCC introduction, even at low filler amounts, while DSC measurements demonstrated that the glass transition temperature progressively increases with the MCC content. Interestingly, DMTA analysis revealed a stabilizing effect on the material produced by microcellulose addition, with an increase of the storage modulus and a decrease of the thermal expansion coefficient, in proportion to the filler loading. Moreover, MCC addition determined an increase of the elastic modulus and creep stability with respect to the neat resin, and an enhancement of fracture toughness (K_{IC}).

Introduction

The use of synthetic resins in the artworks conservation field is linked to their good handling properties, in particular, their flexibility and transparency. Several polymers are used as binding and retouching media, agglutinants, adhesives, consolidants, coating materials, varnishes, or additions for missing parts of an artwork [1, 2].

In particular, acrylic/methacrylic polymers have been used as picture varnishes, since the late of 1930s. Conservative treatments with acrylic resins are carried out for wood, paper, mosaics, pigments, lacquerwares, amber, fossils, ceramics, glass, and stones [3–5]. Paraloid B72®, a methyl-acrylate/ethylene–methyl-acrylate–(MA/EMA) copolymer, is one of the most used thermoplastic resin in restoration. This MA/EMA copolymer, thanks to its capacity of forming soft high transparency coherent films has always been used for metal aerosols, wood coatings, clear coatings for general product finishing, and flexographic printing inks then oriented to artwork restoration as well. Paraloid B72 is suitable as a protective layer for metals and other compact surfaces; as a consolidant by impregnation, of porous materials, such as wooden objects, plasterwork and tuff, and as an adhesive for glasses and ceramics. Moreover, this product is applied in form of solution in the restoration of oil paintings, making a transparent varnish layer and as adhesive in the lining of canvas. Several years of usage of Paraloid B72 and repeated testing of artificial and natural aging demonstrated its higher chemical stability, yellowing resistance, and photothermal oxidation stability with respect other commonly used acrylics resins for art conservation [6–8]. On the other hand, the most severe limitations in the use of acrylics resins are related to their application mode, the resin concentration, and the service conditions. However, these limitations have not impeded the use of Paraloid B72 also in treated surfaces exposed to high humidity and temperature conditions [9]. For the mechanical performances are concerned, Paraloid B72 has been always tested in solution with acetone and/or xylene, or in combination with other polymers (such as a poly-2-ethyl-oxazoline) [10–12].

A. Cataldi (✉) · A. Dorigato · F. Deflorian · A. Pegoretti
Department of Industrial Engineering and INSTM Unit, University of Trento, Via Mesiano 77, 38123 Trento, Italy
e-mail: annalisa.cataldi@ing.unitn.it

Considering the recent attention of composite scientists toward cellulose-based fibers reinforcements as renewable alternative to their synthetic equivalents, microcrystalline cellulose (MCC) was chosen as filler in this work [13, 14]. MCC is obtained in industrial scale from wood and cotton cellulose, but production from materials such as water hyacinth, coconut shells [15], sugar cane bagasse [16], and jute has been investigated as well.

MCC is one of the most used reinforcing fillers, it can be easily prepared through the reaction of cellulose with water solution of strong mineral acid at boiling temperature. The hydrolysis reaction removes the amorphous fraction and reduces the degree of polymerization [level off degree of polymerization (LODP)] of the cellulose chains [17]. Due to the high degree of crystallinity, MCC is not swollen in water, stable at elevated temperature, and under different pH conditions [18, 19]. These natural fibers present several advantages in comparison to synthetic fillers. They are non-toxic, biodegradable, and recyclable. Natural plant derived fibers have generally lower density and high specific strength and elevated stiffness. For this reason, they are applied in the production of low density composites at high filler concentration [20].

The aim of this work is the investigation of the thermo-mechanical properties of thermoplastic composites for the cultural heritage protection made by an acrylic resin (Paraloid B72) and different amounts of a natural filler (MCC). The goal is the improvement of thermo-mechanical performance of this polymer, developing a new microcomposite with specific features more suitable for the specific application (art conservation) and with a lower environmental impact.

Experimental

MCC (Sigma-Aldrich, USA), with a specific gravity of 1.56 g cm^{-3}, was selected as reinforcing filler. According to environmental scanning electron microscope (ESEM) observations (Fig. 1), MCC particles consist of elongated flakes having an average length (L) of about 24 μm and a diameter (D) of about 10 μm (average L/D ratio of 2.4). Paraloid B72 (PB72) resin (Rohm and Hass, Germany) with a specific gravity of 1.15 g cm^{-3} was used as polymer matrix.

Before being process, both microfiller powder and matrix pellets were dried under vacuum at 105 °C for 24 h. Materials were melt compounded in a Haake Rheomix® internal mixer (T = 160 °C, rotor speed = 60 rpm, residence time = 5 min) and compression molded at 170 °C in a Carver hydraulic press under a pressure of 4 MPa for 5 min. Square sheets of neat PB72 and composite samples with a filler amount between 5 and 30 wt%, 150 mm long, and 1.3 mm thick, were prepared. After processing, all samples were stored in sealed bags in vacuum in order to avoid water uptake. Samples were denoted indicating the matrix (PB72), the filler (MCC), and its weight concentration. For instance, PB72-MCC-30 indicates the composite sample with a MCC amount of 30 wt%.

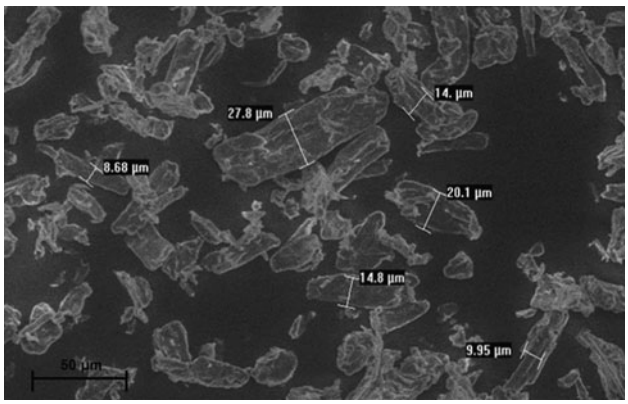

Fig. 1 ESEM image of MCC particles

Microstructural observations on neat MCC powder and on cryofractured surfaces of composites samples were carried out by a Philips XL30 ESEM with an accelerating voltage of 10 kV. The dimensional distribution of MCC powder before and after melt compounding process was evaluated through a Wild Heerbrugg Leica optical microscope. To this scope, small pieces of PB72-MCC-30 sample were dissolved in acetone at 30 °C for 1 h, and the resulting flakes were then dried under vacuum at 105 °C for 2 h. At least 200 measurements were performed on the resulting micrographs by an image analysis software (ImageJ®).

Differential scanning calorimetry (DSC) measurements were performed by using a Mettler Toledo TC15 calorimeter. Samples of about 12 mg were analyzed under a nitrogen flow of 150 ml min^{-1}, applying a first heating stage from 0 to 250 °C linked to a cooling stage from 250 to 0 °C, and to a second heating stage until 250 °C at 10 °C min^{-1}. The glass transition temperature (T_g) was evaluated as the inflection point in the thermograms. Thermal stability of the composites was investigated through thermogravimetric analysis (TGA), by using a Mettler TG50 thermobalance in a temperature interval between 40 and 700 °C, at a heating rate of 10 °C min^{-1}, and under a nitrogen flow of 150 ml min^{-1}. The onset temperature (i.e., the temperature associated to a mass loss of 5 %) and the residual mass at 700 °C were determined. The maximum degradation temperature was evaluated from the peak of mass loss rate curve.

Dynamic mechanical thermal analysis (DMTA) was performed by using DMA Q800 device by TA Instruments under tensile configuration. Rectangular specimens

15 mm long, 5 mm wide, and 1.2 mm thick were tested in a temperature range between −10 and 150 °C at a heating rate of 3 °C min^{-1} and a frequency of 1 Hz. At least three specimens for each composition were tested by DMTA analysis. To assure a linear viscoelastic behavior, the strain amplitude was fixed at 0.05 %. The trends of the storage modulus (E'), loss modulus (E''), and loss tangent (tan δ) as a function of the temperature were registered. Moreover, through the evaluation of the thermal strain it was possible to determine the coefficients of linear thermal expansion (CLTE) below T_g (i.e., in a temperature interval between 0 and 40 °C) and above T_g (between 50 and 55 °C).

Quasi-static tensile tests were carried out on ISO 527 type 1BA samples (gage length 30 mm, width 5 mm, distance between the grips 55 mm, thickness 1.2 mm) by means of an Instron® 4502 universal testing machine, equipped with a 1 kN load cell. Tensile tests for the evaluation of the elastic modulus were performed at a crosshead speed of 0.25 mm min^{-1} (strain rate equal to 0.02 min^{-1}) imposing a maximum axial deformation level of 1 %. The strain was recorded by using a resistance extensometer Instron® model 2620-601 (gage length of 12.5 mm). According to ISO 527 standard, the elastic modulus was evaluated at room temperature as a secant value between deformation levels of 0.05 and 0.25 %. Tensile properties at break were determined by tensile tests at break, executed at room temperature at a crosshead speed of 10 mm min^{-1}, without using the extensometer. At least five specimens were tested for each sample. Flexural tests for the evaluation of the fracture behavior were performed on neat matrix, PB72-MCC-5, and PB72-MCC-30 samples by using the same universal testing machine, equipped with a 1 kN load cell. According to ASTM D 5045 standard, single edge notched bending samples (SENB), 35 mm long, 8 mm wide, and 4 mm thick were tested at a crosshead speed of 10 mm min^{-1}. Samples were pre-notched with a notch depth of 4 mm, producing a notch tip radius of <10 μm. Both critical stress intensity factor (K_{IC}) and critical strain energy release rate (G_{IC}) values were determined as an average value on at least five specimens.

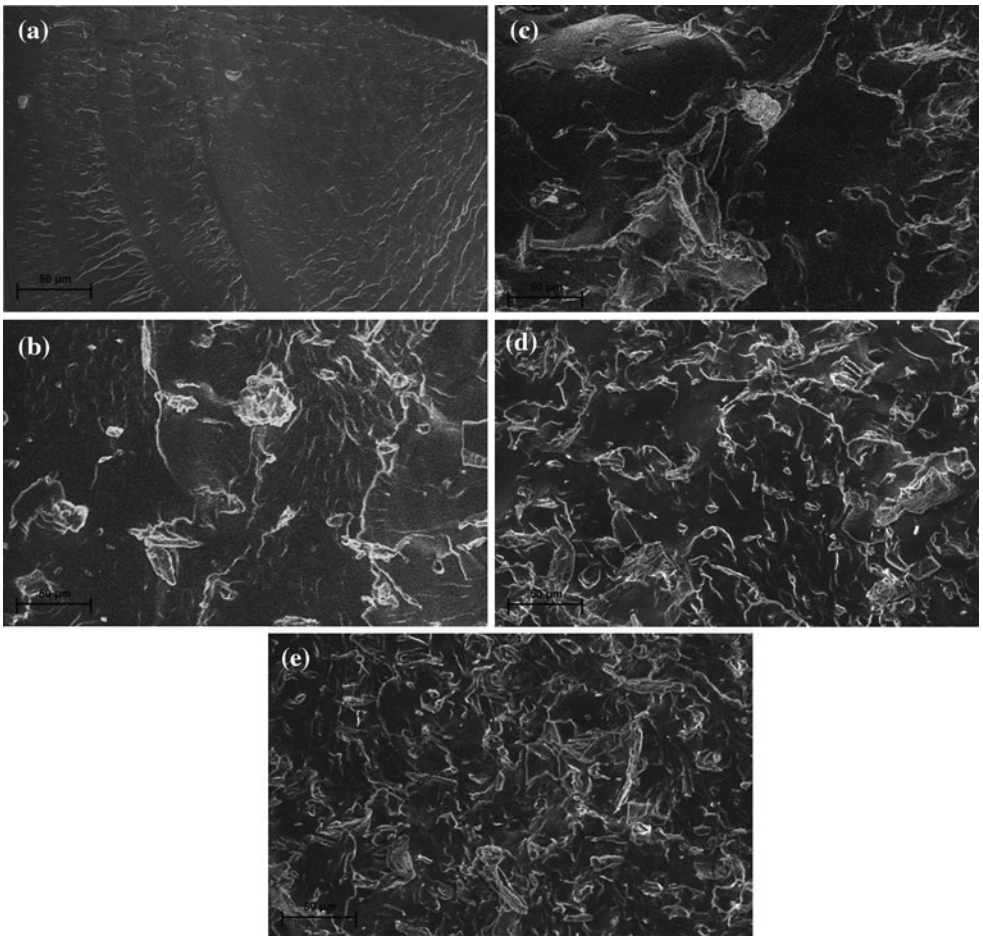

Fig. 2 ESEM images of the cryofractured surfaces of neat PB72 and relative composites. **a** PB72, **b** PB72-MCC-5, **c** PB72-MCC-10, **d** PB72-MCC-20, and **e** PB72-MCC-30

Creep tests were conducted through a DMA Q800 device by TA Instruments under tensile configuration at 30 °C, applying a constant stress (σ_0) of 2.3 MPa, corresponding to about 10 % of the stress at break of neat PB72, for a total time of 3600 s. Rectangular specimens (15 mm long, 5 mm wide, and 1.2 mm thick) were tested and the creep compliance $D(t)$, determined as the ratio between the time dependent deformation $\varepsilon(t)$ and the applied stress (σ_0). Moreover, a creep rate (dD/dt), was estimated as a time derivative of the creep compliance curves.

Results and discussion

Through ESEM micrographs of the cryofractured surfaces of the samples it was possible to evaluate the dispersion degree of MCC flakes within the matrix. As reported in Fig. 2a, the relatively flat cryofractured section of neat PB72 is typical of a brittle material. On the other hand, from the micrographs of composite samples (Fig. 2b–e) it is possible to notice that MCC flakes are uniformly dispersed within the matrix without any preferential direction. In PB72-MCC-5 samples, individual flakes can be detected without a substantial filler aggregation. Moreover, the roughness of the fracture surfaces increases with the MCC content, making difficult a clear detection of MCC flakes. According to literature indications [21, 22], an increase of the surface roughness is generally associated to an increase of the fracture propagation resistance of the material. In any case, a good interfacial adhesion, without evident debonding phenomena, can be observed for all the tested specimens.

It is well-known that the reinforcing capability of the filler in the composites is strictly related to the filler size and to its aspect ratio. Therefore, it could be important to evaluate possible dimensional variation of the filler size induced by the melt compounding process. In Fig. 3a–c, the dimensional distributions of the length, width, and aspect ratio of MCC, obtained by an analysis of optical microscope images of fibers extracted from solubilized composites (not reported here for the sake of brevity) are reported. Considering the experimental error associated to these measurements, it can be concluded that the processing step does not markedly reduced the average dimensions of the MCC particles in the composites. As reported in the literature, natural fibers can maintain their specific aspect ratio during melt processing thanks to their high flexibility [23, 24]. Interestingly, after melt compounding, the size distribution of the MCC flakes is slightly broader with a fraction of particles having higher size with respect to the un-compounded flakes. This aspect could be explained considering the mechanical deformation induced at elevated temperature by the rotors

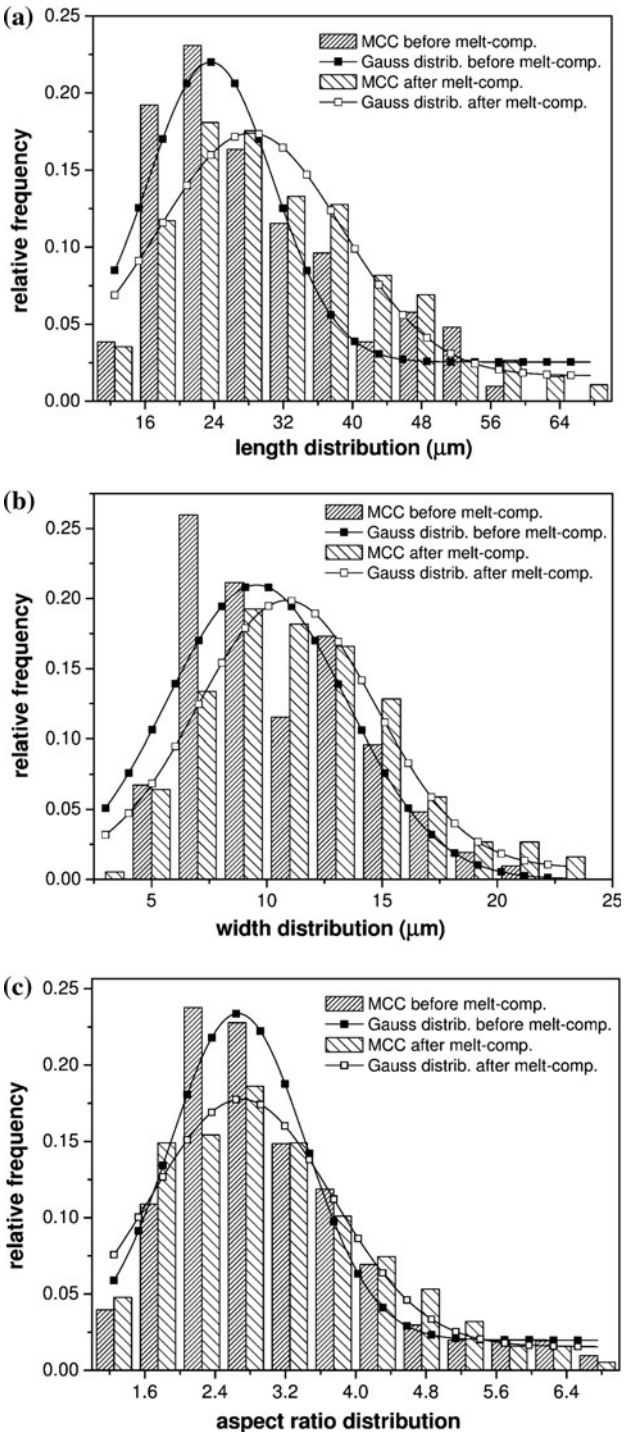

Fig. 3 MCC size distribution before and after processing cycle. **a** Length distribution, **b** width distribution, and **c** aspect ratio distribution

of the melt compounder and/or the hot pressing on the MCC particles.

In Fig. 4 DSC thermograms of neat PB72 and relative composites collected during the first heating stage are reported. All specimens show the typical trend of amorphous polymer, with the presence of an inflection point at

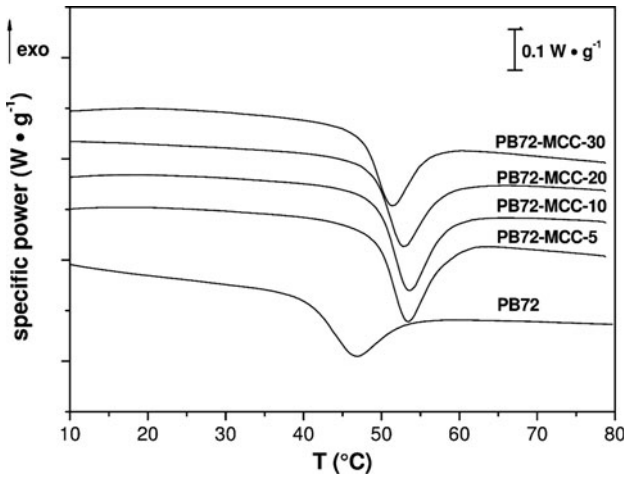

Fig. 4 DSC thermograms of neat PB72 and relative composites (first heating stage)

Table 1 Glass transition temperature (T_g) of neat PB72 and relative composites from DSC tests (first heating stage)

Samples	T_g (°C)		
	First heating	Cooling	Second heating
PB72	40.5	31.4	39.8
PB72-MCC-5	48.4	34.0	42.6
PB72-MCC-10	46.7	35.6	41.9
PB72-MCC-20	47.9	34.7	40.9
PB72-MCC-30	46.5	33.0	41.0

around 40 °C, due to the glass transition temperature. In Table 1, glass transition temperatures of each sample collected during heating and cooling stages are summarized. In the first heating, it is possible to note that MCC introduction leads to a glass transition temperature increase, proportionally with the filler concentration. For instance, PB72-MCC-30 presents a T_g enhancement of about 7 °C with respect to the neat resin. Considering that the dimensional stability at elevated temperature of amorphous polymers depends on their glass transition temperature, it can be concluded that MCC introduction could be particularly useful to increase the maximum service temperature of these materials. On the other hand, cooling and second heating scans reported no relevant variation of the T_g with increasing of MCC content.

TGA thermograms of the constituents and of the relative composites are reported, in Fig. 5a, while in Fig. 5b the derivative of the mass loss curves is represented. The most important parameters regarding the thermal stability of the investigated materials are summarized in Table 2. Even though the degradation resistance of MCC flakes is lower than the neat PB72 matrix one, all composite samples show an interesting improvement of the onset degradation

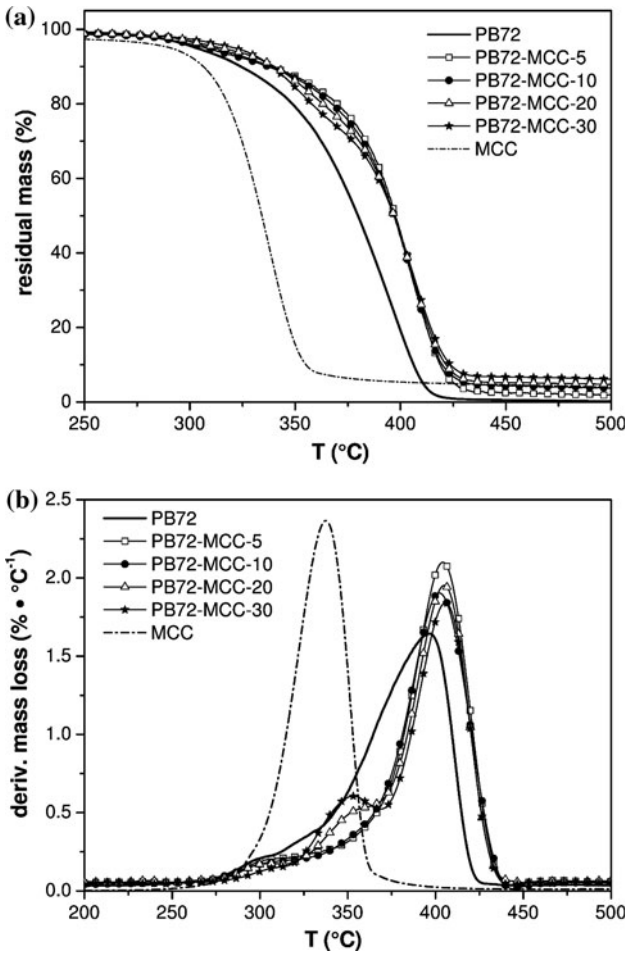

Fig. 5 TGA thermograms of neat PB72, neat MCC, and relative composites. **a** Residual mass as a function of temperature and **b** derivative of the mass loss

Table 2 Results of TGA test on neat PB72, MCC and relative composites

Samples	T_{onset} (°C)	T_{max} (°C)	Residual mass at 700 °C (%)
PB72	298	396	–
PB72-MCC-5	310	406	0.2
PB72-MCC-10	308	406	1.0
PB72-MCC-20	314	406	2.2
PB72-MCC-30	321	406	3.4
MCC	291	337	0.8

T_{onset} temperature of the initial degradation step (corresponding to a mass loss of 5 wt%), T_{max} temperature of the maximum degradation rate

temperature (T_{onset}) and of the temperature associated to the maximum mass loss rate (T_{max}). According to widely accepted explanation [25], the introduction of filler in polymeric materials can promote the formation of char enriched surface layer during the combustion, limiting the diffusion of the oxidant species through the samples, and

inhibiting the degradation process. This effect is particularly evident in nanofilled composites, but it could be found also in some microcomposites. This hypothesis is confirmed by the fact that the residual mass at 700 °C increases proportionally to the filler content. Once again, this could be due to the formation of a ceramized surface layer on the samples, which does not allow a complete combustion and vaporization of the matrix. From mass loss rate curves reported in Fig. 5b one can notice the presence of a first degradation step at 350 °C for the composites at elevated filler amount. Although this first degradation peak was detected in other studies on MCC polymer composites [26], it is difficult to assess if it could be attributed to a fraction of MCC particles that starts to degrade immediately after the main degradation stage of neat MCC particles or if it is due to an early degradation of a fraction of PB72 matrix induced by the presence of the microcellulose filler.

The temperature dependence of the storage modulus, loss modulus, loss tangent, and thermal strain curves of neat PB72 and relative composites, obtained from DMTA analysis, is

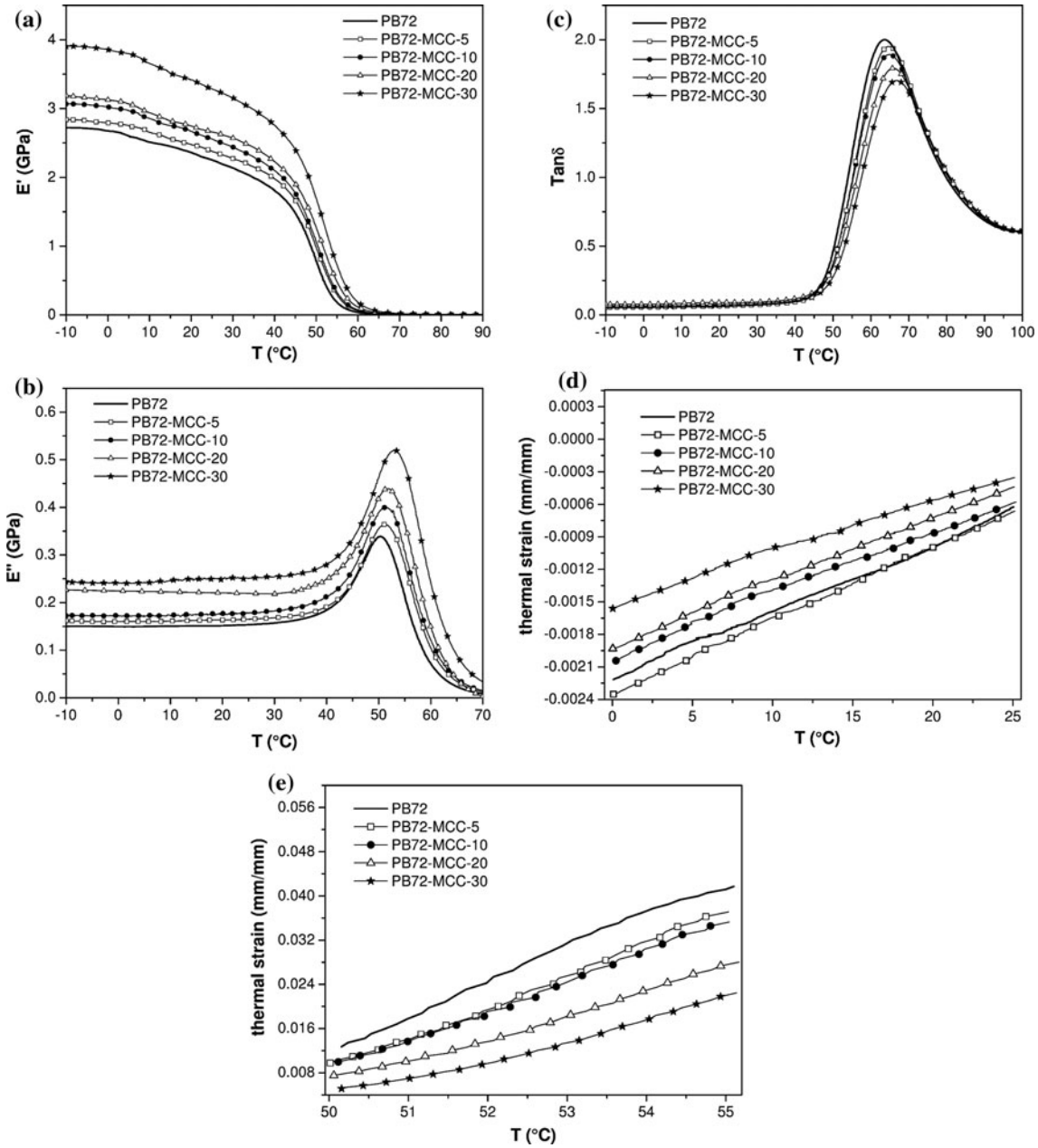

Fig. 6 DMTA on neat PB72 and relative composites ($f = 1$ Hz). **a** Storage modulus, **b** loss modulus, **c** loss factor, **d** thermal strain below glass transition temperature, and **e** thermal strain above glass transition temperature

Table 3 Results of DMTA tests on neat PB72 and relative composites

Samples	E' at 0 °C (GPa)	E' at 30 °C (GPa)	E' at 60 °C (GPa)	T_g (E'' peak) (°C)	T_g (tan δ peak) (°C)	$CLTE_g$ (K^{-1})	$CLTE_r$ (K^{-1})
PB72	2.68 ± 0.04	2.14 ± 0.05	0.04 ± 0.02	50.5 ± 0.2	62.9 ± 0.3	6.3E−05 ± 0.1	6.2E−03 ± 0.2
PB72-MCC-5	2.79 ± 0.02	2.27 ± 0.03	0.06 ± 0.01	51.3 ± 0.1	64.3 ± 0.1	6.7E−05 ± 0.1	5.7E−03 ± 0.2
PB72-MCC-10	3.02 ± 0.02	2.44 ± 0.02	0.07 ± 0.03	51.4 ± 0.1	64.1 ± 0.2	5.7E−05 ± 0.1	5.4E−03 ± 0.1
PB72-MCC-20	3.13 ± 0.03	2.57 ± 0.01	0.12 ± 0.02	51.8 ± 0.2	65.3 ± 0.2	5.8E−05 ± 0.1	4.2E−03 ± 0.1
PB72-MCC-30	3.86 ± 0.02	3.16 ± 0.01	0.19 ± 0.02	52.9 ± 0.1	65.9 ± 0.1	4.8E−05 ± 0.1	3.6E−03 ± 0.1

E' storage modulus at different temperatures, T_g glass transition temperature, $CLTE_g$ coefficient of linear thermal expansion in the glassy state (interval 0–25 °C), $CLTE_r$ coefficient of linear thermal expansion in the rubbery state (interval 50–55 °C)

reported in Fig. 6a–d, while in Table 3, the some relevant parameters are summarized. First of all, both the storage (E') and the loss (E'') moduli increase proportionally to the filler loading. Correspondingly, tan δ values decrease as the MCC content increases. This stabilizing effect due to MCC introduction has been already reported in other literature studies [13, 26, 27]. According to DMTA tests, the temperatures associated to E'' and tan δ peaks (representing the glass transition temperature of the system) slightly shift toward higher values (about 3°). In addition, the CLTE was calculated as the slope of the secant line of thermal strain curves in the glassy ($CLTE_g$ between 0 and 25 °C) or rubbery ($CLTE_g$ between 50 and 55 °C) states, according to Eq. (1):

$$\mathrm{CLTE} = \frac{\Delta L}{L_0 \cdot \Delta T}, \tag{1}$$

where L_0 is the original length of the samples (i.e., the length of the samples at 0 or at 50 °C), ΔL is the thermal displacement in the considered temperature interval (ΔT). Interestingly, as reported in Table 3, the introduction of MCC flakes in the matrix induces a general reduction of the CLTE with the filler loading both under and above the glass transition temperature. This improvement could be particularly important for the dimensional stability of artwork protecting agents based on PB72 resins.

Representative stress/strain curves obtained from quasi-static tensile tests of neat PB72 and of the relative composites are reported in Fig. 7a, while in Table 4 the most important parameters obtainable from the curves are summarized. Tensile tests clearly evidence a progressive increase of the elastic modulus (E) with the filler loading. In order to better understand elastic properties of examined samples, a modeling of the experimental elastic modulus data was attempted. Elastic modulus data were fitted by using an empirical model traditionally used for composites with short fibers reinforced randomly oriented in a plane [28]. According to Eq. (2), the tensile modulus of 2D randomly oriented fibers composites (E_C) can be related to the elastic moduli of ideal composites having the same volume fraction of fibers perfectly aligned (E_L) or transversally oriented (E_T) to the loading axis:

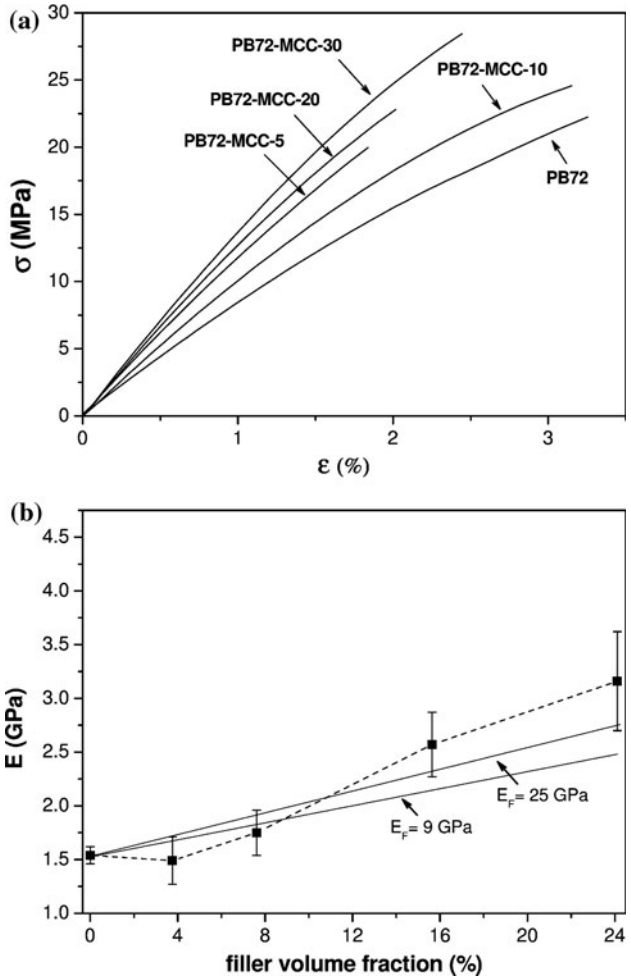

Fig. 7 Quasi-static tensile tests of neat PB72 and relative composites. **a** Representative stress–strain curves, and **b** elastic modulus trend, with theoretical predictions according to Eq. (2) (*full lines*)

$$E_C = \frac{3}{8}E_L + \frac{5}{8}E_T. \tag{2}$$

The moduli (E_L, E_T) can be calculated by using Halpin–Tsai model [29] according to the following equations:

Table 4 Mechanical properties of neat PB72 and relative composites

Samples	E (GPa)	σ_b (MPa)	ε_b (%)	TEB (MJ m^{-3})	K_{IC} (MPa $m^{1/2}$)	G_{IC} (KJ m^{-2})
PB72	1.54 ± 0.08	23.01 ± 1.51	3.46 ± 0.19	0.44 ± 0.08	0.55 ± 0.03	0.011 ± 0.001
PB72-MCC-5	1.49 ± 0.22	21.22 ± 2.37	2.28 ± 0.43	0.34 ± 0.11	0.59 ± 0.02	0.016 ± 0.003
PB72-MCC-10	1.75 ± 0.21	23.14 ± 2.09	2.98 ± 0.31	0.40 ± 0.06	–	–
PB72-MCC-20	2.57 ± 0.30	23.80 ± 2.27	2.14 ± 0.28	0.28 ± 0.07	–	–
PB72-MCC-30	3.32 ± 0.40	26.02 ± 2.44	2.09 ± 0.33	0.35 ± 0.09	0.99 ± 0.03	0.031 ± 0.002

E elastic modulus, σ_b stress at break, ε_b strain at break, *TEB* tensile energy to break, K_{IC} critical stress intensity factor, G_{IC} critical strain energy release rate

$$E_L = \frac{1 + 2(L/D)(\eta_L \phi)}{1 - \eta_L \phi} E_M, \quad (3)$$

$$E_T = \frac{1 + 2\eta_T \phi}{1 - \eta_T \phi} E_M, \quad (4)$$

and:

$$\eta_L = \frac{(E_F/E_M) - 1}{(E_F/E_M) + 2(L/D)}, \quad (5a)$$

$$\eta_T = \frac{(E_F/E_M) - 1}{(E_F/E_M) + 2}, \quad (5b)$$

where L/D is the aspect ratio of the fibers, Φ is the volume fraction of the fibers, and E_F and E_M are the fibers and matrix moduli, respectively. The comparison between the experimental values of the moduli of composites under investigation and the values predicted according to Eq. 2 are compared in Fig. 7b. Two theoretical predictions were considered, by using two different MCC elastic modulus values. The first one (i.e., 9.2 GPa) was determined by Hancock et al. [30] through micromechanical tests, while the second one (i.e., 25 GPa) was estimated by Eichorn and Young [31] through Raman spectroscopy. Considering standard deviation values, one can see that the proposed model is able to satisfactorily fit experimental data until a MCC content of 20 wt%, regardless to the MCC elastic modulus value. While for the highest filler amount, the predicted moduli by Halpin–Tsai equation are lower than the experimental one. Another important experimental evidence is that stress at break is not substantially affected by MCC addition, while strain at break is slightly reduced. This slight drop in strain at break can induce a limited decrease of the specific tensile energy to break (TEB) values as the filler increases (see Table 4).

On the basis of these results, neat PB72, PB72-MCC-5, and PB72-MCC-30 composites were selected for a deeper investigation of their fracture behavior, based on the determination of linear elastic fracture parameters K_{IC} and G_{IC}. In Fig. 8, representative force–displacement curves obtained from flexural tests on SENB samples are reported, while in Table 4, K_{IC} and G_{IC} values are listed. It is

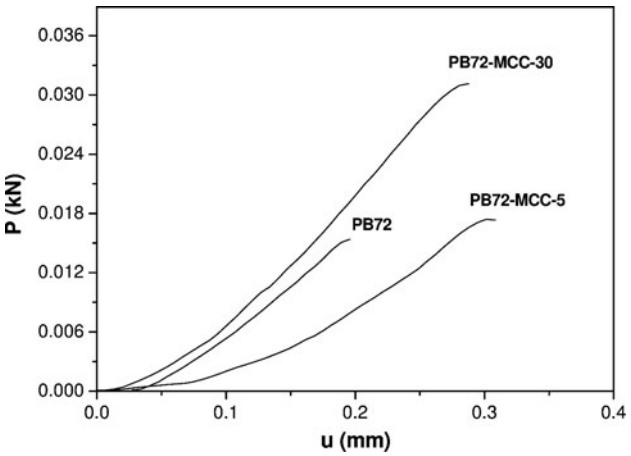

Fig. 8 Representative load–displacement curves from flexural test for the determination of K_{IC} and G_{IC} of neat PB72 and relative composites

interesting to note that both the fracture toughness parameters are noticeably increased upon MCC addition: K_{IC} increases from 0.55 MPa $m^{1/2}$ for the neat matrix to 0.99 MPa $m^{1/2}$ for PB72-MCC-30 sample, while G_{IC} value increases from 0.01 to 0.03 kJ m^{-2}. Therefore, even if quasi-static tensile test evidenced a slight reduction of the TEB values, MCC introduction determined a substantial improvement of the fracture resistance of the material. In quasi-static tensile tests on un-notched samples, the presence of MCC microparticles could be responsible of the stress concentration and of the crack nucleation, while when a notch is already present on the sample the embrittling effect due to MCC is not effective and other mechanisms can be responsible of the toughening effect encountered for filled samples. It could be tentatively hypothesized that the presence of MCC microflakes modify the crack propagation path, with positive effects on the fracture toughness of the material.

The stabilizing effect provided by MCC flakes is confirmed by creep test. In fact, as reported in Fig. 9a, creep compliance is significantly reduced at elevated filler contents, especially for long creep times. It is interesting to note that also creep rate values in the secondary creep stage

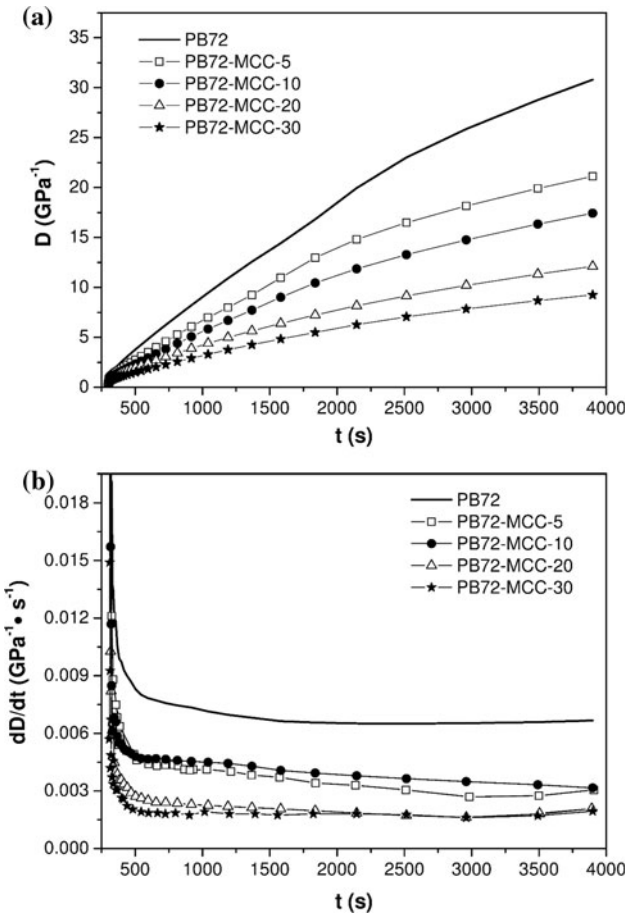

Fig. 9 Creep behavior of neat PB72 and relative composites. **a** Creep compliance curves and **b** creep rate curves

are progressively reduced as the MCC content increases (Fig. 9b). This aspect could play a positive role for those applications where a good dimensional stability of the consolidant resin is required (i.e., lining of oil painting canvas under constant long-lasting stress conditions).

Conclusions

Different amounts of MCC were melt compounded with a commercial MA/EMA acrylate matrix to be used in artwork restoration field, in order to investigate their effect on the thermo-mechanical behavior of the resulting materials.

Glass transition temperature of PB72 matrix is enhanced with increasing the MCC loading, while TGA tests revealed that MCC addition lead to an increase of thermal degradation stability with the neat matrix. Interestingly, an increase of storage modulus and loss modulus proportionally to the MCC loading was detected, evidence of a stabilizing effect due to the MCC introduction and a good filler/matrix affinity. Moreover, a remarkable reduction of linear coefficient of thermal expansion in the whole range of tested temperature interval was highlighted. Tensile tests confirmed the stiffening effect induced by MCC, with an increase of the elastic modulus. Also creep compliance values are considerably reduced upon MCC addition. The fracture propagation resistance of PB72 is considerably improved by MCC addition, with a progressive improvement both of the K_{IC} and G_{IC} values.

Concluding, addition of MCC could represent an effective way to improve the thermo-mechanical behavior of a commercial acrylate widely used in the art conservation field, especially for those consolidation purposes where elevated dimensional stability and a good energy absorption capability under external loads are required.

References

1. Mills JS, White R (1994) The organic chemistry of museum objects, 2nd edn. Butterworth, Oxford
2. Van Oosten T, Shashoua Y, Waentig F (2002) Plastics in arts: history, technology, preservation. Kölner Beiträge zur Restaurierung und Konservierung von Kunst- und Kulturgut Band 15. Siegl, Munich
3. Robson M (1992) Early advances in the use of acrylic resins for the conservation of antiquities. In: Allen NS, Edge M, Horie CV (eds) Polymers in conservation. Royal Society of Chemistry, Cambridge, p 184
4. Taylor TH (1984) In situ repair of architectural glass, adhesives and consolidants. International Institute for Conservation, London
5. Amoroso GG, Fassina V (1973) Stone decay and conservation. Elsevier, Amsterdam
6. Chiantore O, Lazzari M (2001) Photo-oxidative stability of paraloid acrylic protective polymers. Polymer 42(1):17–27
7. Lazzari M, Chiantore O (2000) Thermal-ageing of paraloid acrylic protective polymers. Polymer 41(17):6447–6455
8. Sale D (2011) Yellowing and appearance of conservation adhesives for poly(methyl methacrylate): a reappraisal of 20-year-old samples and test methods. In: Adhesives and consolidants for conservation, Ottawa
9. Chapman S, Mason D (2003) Literature review: the use of Paraloid B-72 as a surface consolidant for stained glass. J Am Inst Conserv 42(11):381–392
10. Down JL, MacDonald MA, Tétreault J, Williams RS (1996) Adhesive testing at the Canadian Conservation Institute: an evaluation of selected poly(vinyl acetate) and acrylic adhesives. Stud Conserv 41(1):19–44
11. Hansen EF, Derrick MR, Schilling MR, Garcia R (1991) The effects of solution application on some mechanical and physical properties of thermoplastic amorphous polymers used in conservation: poly(vinyl acetate)s. J Am Inst Conserv 30(2):203–213
12. Keskkula H, Paul DR (1986) Miscibility of polyethyloxazoline with thermoplastic polymers. J Appl Polym Sci 31(5):1189–1197
13. Spoljaric S, Genovese A, Shanks RA (2009) Polypropylene–microcrystalline cellulose composites with enhanced compatibility and properties. Composites A 40(6–7):791–799
14. Shanks RA, Hodzic A, Ridderhof D (2006) Composites of poly(lactic acid) with flax fibers modified by interstital polymerization. J Appl Polym Sci 99(23):5–13

15. Gaonkar SM, Kulkarni PR (1989) Microcrystalline cellulose from coconut shells. Acta Polym 40(4):292–294
16. Padmadisastra Y, Gonda I (1989) Preliminary studies of the development of a direct compression cellulose excipient from bagasse. J Pharm Sci 78(6):508–514
17. Thummanukitcharoen P, Limpanart S, Srikulkit K (2011) Preparation of organosilane treated microcrystalline cellulose (SIMCC) and the polypropylene/SIMCC composite. In: 18th International conference on composite materials, Jeju Island
18. Chauhan YP, Sapkal RS, Sapkal VS, Zamre GS (2009) Microcrystalline cellulose from cotton rags (waste from garment and hosiery industries). Int J Chem Sci 7(2):681–688
19. Das K, Ray D, Bandyopadhyay NR, Sengupta S (2010) Study of the properties of microcrystalline cellulose particles from different renewable resources by XRD, FTIR, nanoindentation, TGA and SEM. J Polym Environ 18(3):355–363
20. Qui W, Endo T, Hirotsu T (2006) Interfacial interaction, morphology and tensile properties of a composite of highly crystalline cellulose and maleated polypropylene. J Appl Polym Sci 102(38):30–41
21. Dorigato A, D'Amato M, Pegoretti A (2012) Thermo-mechanical properties of high density polyethylene—fumed silica nanocomposites: effect of filler surface area and treatment. J Polym Res 19:9889–9899
22. Dorigato A, Pegoretti A, Quaresimin M (2011) Thermo-mechanical characterization of epoxy/clay nanocomposites as matrices for carbon/nanoclay/epoxy laminates. Mater Sci Eng A 528:6324–6333
23. Bledzki AK, Gassan J (1999) Composites reinforced with cellulose based fibres. Prog Polym Sci 24:221–274
24. Kalaitzidou K, Fukushima H, Drzal LT (2007) Mechanical properties and morphological characterization of exfoliated graphite–polypropylene nanocomposites. Composites A 38:1675–1682
25. Dorigato A, Morandi S, Pegoretti A (2012) Effect of nanoclay addition on the fiber/matrix adhesion in epoxy/glass composites. J Compos Mater 46:1439–1451
26. Kiziltas A, Gardner DJ, Han Y, Yang HS (2011) Dynamic mechanical behavior and thermal properties of microcrystalline cellulose (MCC)-filled nylon 6 composites. Thermochim Acta 519(1–2):38–43
27. Mathew AP, Oksman K, Sain MM (2005) Mechanical properties of biodegradable composites from poly lactic acid (PLA) and microcrystalline cellulose (MCC). J Appl Polym Sci 97:2014–2025
28. Lavengood RE, Goettler LA (1971) Stiffness of non-aligned fiber reinforced composites. US Government R&D Reports, vol AD886372. National Technical Information Service, Springfield
29. Halpin JC (1969) Stiffness and expansion estimates for oriented short fibre composites. J Compos Mater 3:732–735
30. Hancock BC, Clas S-D, Christensen K (2000) Micro-scale measurement of the mechanical properties of compressed pharmaceutical powders. 1: the elasticity and fracture behavior of microcrystalline cellulose. Int J Pharm 209(1–2):27–35
31. Eichhorn SJ, Young RJ (2001) The young's modulus of a microcrystalline cellulose. Cellulose 8:197–207